Polymer 50 (2009) 2492–2502

Contents lists available at ScienceDirect

Polymer

journal homepage: www.elsevier.com/locate/polymer

Polyamide- and polycarbonate-based nanocomposites prepared from thermally stable imidazolium organoclay

Lili Cui [a], Jason E. Bara [b], Yefim Brun [c], Youngjae Yoo [a], P.J. Yoon [d], D.R. Paul [a,*]

[a] Department of Chemical Engineering and Texas Materials Institute, The University of Texas at Austin, Austin, TX 78712, USA
[b] Department of Chemical & Biological Engineering, The University of Colorado at Boulder, Boulder, CO 80309, USA
[c] E.I. DuPont Company, Central Research and Development, Wilmington, DE 19880, USA
[d] Southern Clay Products, 1212 Church Street, Gonzales, TX 78629, USA

ARTICLE INFO

Article history:
Received 20 January 2009
Received in revised form
7 March 2009
Accepted 9 March 2009
Available online 28 March 2009

Keywords:
Nanocomposites
Organoclays
Thermal stability

ABSTRACT

This paper explores the possible advantages of the more thermally stable imidazolium-based organoclay over a more conventional ammonium-based organoclay for facilitating exfoliation and minimizing polymer matrix degradation in melt blended polyamide 6 (PA-6) and polycarbonate (PC) nanocomposites. The thermal stability of the two organoclays was evaluated by TGA analyses. The extent of clay exfoliation was judged by analysis of the morphology and tensile modulus of these nanocomposites formed using a DSM Microcompounder, while the extent of color formation and molecular weight change were used to evaluate polymer matrix degradation. For PA-6 and PC nanocomposites, the use of the imidazolium organoclay only produced slight differences in both exfoliation and molecular weight change, although the imidazolium organoclay is remarkably more thermally stable than the ammonium organoclay.

1. Introduction

Melt processing is an attractive approach for forming polymer nanocomposites due to its advantages for commercial production. In this process, the polymer and organoclay are heated to temperatures well above the melting or softening point of the polymer, typically above 200 °C. Thus, for polymers that require high melt processing temperatures, e.g., polyamides and polycarbonates, the thermal stability of the organic component of the modified clay and its impact on the ability to exfoliate the clay platelets plus any consequent effect on the polymer matrix are issues that must be considered. As reported previously [1–3], the traditional ammonium-based organic surfactants used to modify commercial organoclays begin to show measurable thermal degradation at temperatures as low as 180 °C. Prior studies in this laboratory have suggested that the byproducts formed from the breakdown of the organic surfactant might lead to degradation of the polymer during melt processing [2,4]. Imidazolium-type cations have been reported to be much more thermally stable than ammonium-based cations [5–9]. Davis et al. [8] reported some fairly well-exfoliated poly(ethylene terephthalate) nanocomposites with less intensive color formation using an imidazolium surfactant modified organoclay compared to that shown by nanocomposites formed from an ammonium surfactant modified organoclay. The syndiotactic polystyrene (s-PS)/Imidazolium organoclay nanocomposites formed by Manias et al. [10] using a static melt-intercalation method at 290 °C show intercalated morphology and slightly improved thermal stability compared to that of the neat s-PS.

In this study, two organoclays with remarkable differences in thermal stability, based on an imidazolium cation and an ammonium cation where each contains one long alkyl tail, were used to form nanocomposites. Polyamide 6 (PA-6) and polycarbonate (PC) were chosen as the polymer matrices. PA-6 is well known for its capability to form well-exfoliated nanocomposites from organoclays [11–14], while PC is susceptible to a variety of degradation reactions [15–18] during melt blending with commercial organoclays [4]. This paper explores the possible advantages of the more thermally stable imidazolium-based organoclay over a more conventional ammonium-based organoclay for facilitating exfoliation and minimizing polymer matrix degradation and color formation. The extent of clay exfoliation is judged by analysis of the morphology and tensile modulus of the nanocomposites formed using a DSM Microcompounder, while the extent of polymer matrix degradation and color formation experienced during the melt processing of the

* Corresponding author. Tel.: +1 512 471 5392; fax: +1 512 471 0542.
E-mail address: drp@che.utexas.edu (D.R. Paul).

0032-3861/$ – see front matter © 2009 Elsevier Ltd. All rights reserved.
doi:10.1016/j.polymer.2009.03.036

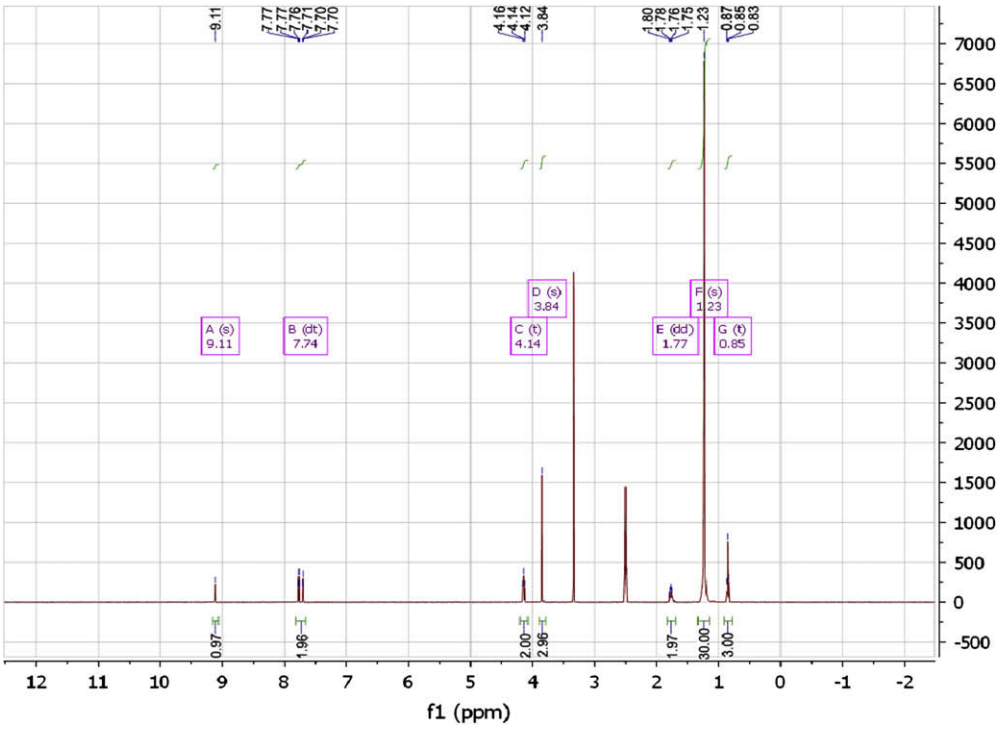

Fig. 1. ^{1}H NMR spectrum of 1-octadecyl-3-methylimidazolium bromide.

nanocomposites are characterized through the determination of the polymer molecular weight and colorimeter measurements.

2. Experimental

2.1. Materials

Two commercial polymers, i.e., Capron B135WP (PA-6) from Honeywell and Iupilon E2000FN (PC) supplied by Mitsubishi Engineering Plastic Corporation, were used in this study to form the two series of melt compounded nanocomposites.

The octadecyl-trimethyl ammonium chloride surfactant used was supplied by Akzo Nobel. The 1-octadecyl-3-methyl imidazolium bromide surfactant was synthesized using chemicals purchased from Sigma–Aldrich (Milwaukee, WI, USA). The chemicals were used as-received with the exception of 1-bromooctadecane, which was received as a dark brown solid. This material was dissolved in *n*-hexane and the solution was passed through a plug of silica. The clear, colorless filtrate was reduced via rotary evaporation and the remaining product was dried under vacuum at 65 °C for several hours. Subsequent cooling to ambient temperature produced a colorless solid. 90.00 g (269.9 mmol) purified 1-bromooctadecane was dissolved in 200 mL toluene, and 19.95 g (243.0 mmol) 1-methylimidazole was added. The reaction was heated at reflux (110 °C) overnight. After this, cooling of the reaction mixture produced a white solid, which was collected and washed with 500 mL Et_2O. 1-Octadecyl-3-methylimidazolium bromide was recrystallized from 700 mL hot EtOAc followed by being dried under vacuum as a fine white powder (Yield = 97.52 g (96.6%)). The imidazolium bromide salt formed is quite pure, as evidenced by the ^{1}H NMR spectrum (400 MHz, DMSO) in Fig. 1. The primary chemical shifts are described as follows: $\delta = 9.11$ (s, 1H), 7.74 (dt, $J = 1.8$, 26.8, 2H), 4.14 (t, $J = 7.2$, 2H), 3.84 (s, 3H), 1.77 (dd, $J = 7.3$, 14.3, 2H), 1.23 (s, 30H), and 0.85 (t, $J = 6.9$, 3H). The peak at 2.50 ppm is DMSO in d_6-DMSO, and the peak at about 3.35 ppm is water in the d_6-DMSO.

The two experimental organoclays based on montmorillonite (see Table 1) were formed at Southern Clay Products, Inc. using a cationic exchange procedure. The aqueous suspension of sodium montmorillonite (CEC = 92 milliequivalent per 100 g) containing ~3% dry clay was heated to 65 °C to promote the cationic exchange reaction, and then was reacted in a stirred tank by pouring 95 milliequivalent of the surfactant based on 100 g of the sodium montmorillonite for 30 min. Then, the flocculated organoclay was transferred to a homogenizer to finish the reaction followed by washing with water and vacuum filtering. The excess water was removed in a convection oven. The dry organoclay was milled to a fine powder which passed through a 0.12 mm screen and subsequently a 0.08 mm screen. Neither of the organoclays formed was subjected to the frequently reported [1,8,19–21] exhaustive purification protocol to remove the excess unreacted surfactant and the byproduct sodium halide of the ion-exchange process. The presence of the residual neucleophilic halide anions usually impair the thermal stability of organoclays [1,5,22], which may consequently contribute to the degradation of the matrix polymer; however, the major difference in the thermal stability of the two organoclays originates from their cation types, and the purity of these organoclays is not the key issue for this investigation.

Table 1
Organoclays used in this study.

Organoclay designation	Surfactant cation structure	
$M_3(C18)_1$	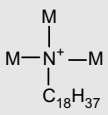	Octadecyl–trimethyl ammonium
Imidazolium $(C18)_1$	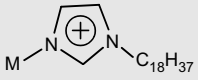	1-Octadecyl-3-methylimidazolium

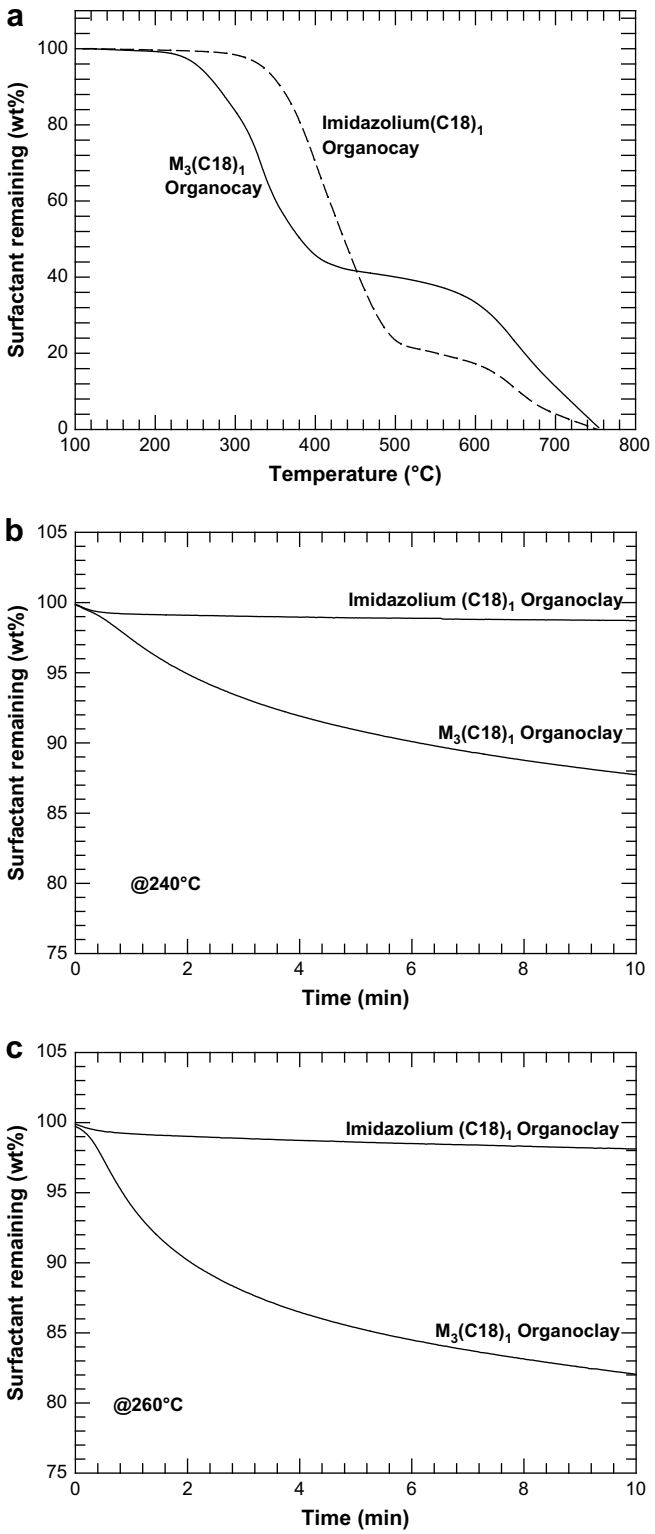

Fig. 2. Comparison of thermal stability by TGA of the two organoclays, $M_3(C18)_1$ and Imidazolium $(C18)_1$: (a) temperature sweeps at 20 °C/min, (b) isothermal at 240 °C, and (c) isothermal at 260 °C.

2.2. Melt processing

PA-6 and PC nanocomposites were prepared by using a DSM 5 melt compounder, which has a net barrel capacity of 5 cm^3, using a screw speed of 100 rpm and with the protection of an extra dry N_2 purge. The barrel temperature was set at 240 °C in the case of nylon 6 and 260 °C for polycarbonate. For both series of nanocomposites, the polymer and organoclay were added at the same time. All materials were dried in a vacuum oven at 80 °C overnight prior to use.

Test bars were formed using a DSM microinjection molding machine with the mold temperature set at 80 °C and the barrel temperature at 245 °C for PA-6 nanocomposites and 265 °C for polycarbonate nanocomposites. The dimensions of the molded specimen were $0.32 \times 1.00 \times 7.10\ cm^3$. The injection molding pressure and holding pressure were both set at 60 bars. The data below are reported in terms of the weight percent montmorillonite (MMT) in the composites rather than the amount of organoclay, since the silicate is the reinforcing component [11,13,23–25].

2.3. Characterization

2.3.1. Morphology

The morphology of the nanocomposites was probed using wide angle X-ray scattering (WAXS) and transmission electron microscopy (TEM). WAXS scans were performed on injection molded rectangular bars, as well as on the organoclay powder, in the reflection mode at a scan rate of 3°/min using a Bruker AXS D8 Advance diffractometer with an incident X-ray wavelength of 1.541 Å. Ultrathin sections, approximately 50 nm in thickness, were cut from the central part of injection molded bars parallel to the flow direction under cryogenic conditions using a RMC PowerTome XL microtome. TEM images were obtained using a JEOL 2010F transmission electron microscope operating at an accelerating voltage of 120 kV.

2.3.2. Modulus

The modulus of the nanocomposites was determined via tensile tests according to ASTM D638 using an Instron model 1137, upgraded for computerized data acquisition, operated at a crosshead speed of 0.51 cm/min using an extensometer. Failure properties were not measured, because dumb-bell shaped specimens could not be prepared by the available molds for the microinjection-molding machine.

2.3.3. TGA

Thermogravimetric analysis (TGA) was carried out on neat organoclays to examine thermal stability. The experiments were conducted using a Perkin–Elmer TGA 7 under nitrogen atmosphere at a gas flow rate of 20 mL/min. Both organoclays were kept in a vacuum oven overnight at 80 °C prior to thermal analysis to remove most of the moisture and volatiles that existed in the organoclay samples. Before performing the TGA tests, the samples were held at 110 °C until their weight stabilized. Two thermal protocols were used: (1) heating at the constant rate of 20 °C/min from 110 °C to 750 °C and (2) heating isothermally at various temperatures.

2.3.4. Color measurements

Color values of injection molded nanocomposite bars were determined in the reflective mode by a colorimeter, MICRO S-5 Brightmeter equipped with a quartz–tungsten–halogen lamp. The CIELAB color values, L^* and YI, which represent the darkness and yellowness of color in the chromaticity coordinates respectively, were computed using a series of formulas described in ASTM E313, and used to quantify differences in color among the various nanocomposites.

2.3.5. Size exclusion chromatography (SEC)

The samples were analyzed by a triple detection SEC system comprised of an Alliance 2695™ Separation Module (Waters Corporation, Milford, MA, USA) with column and sample heaters at

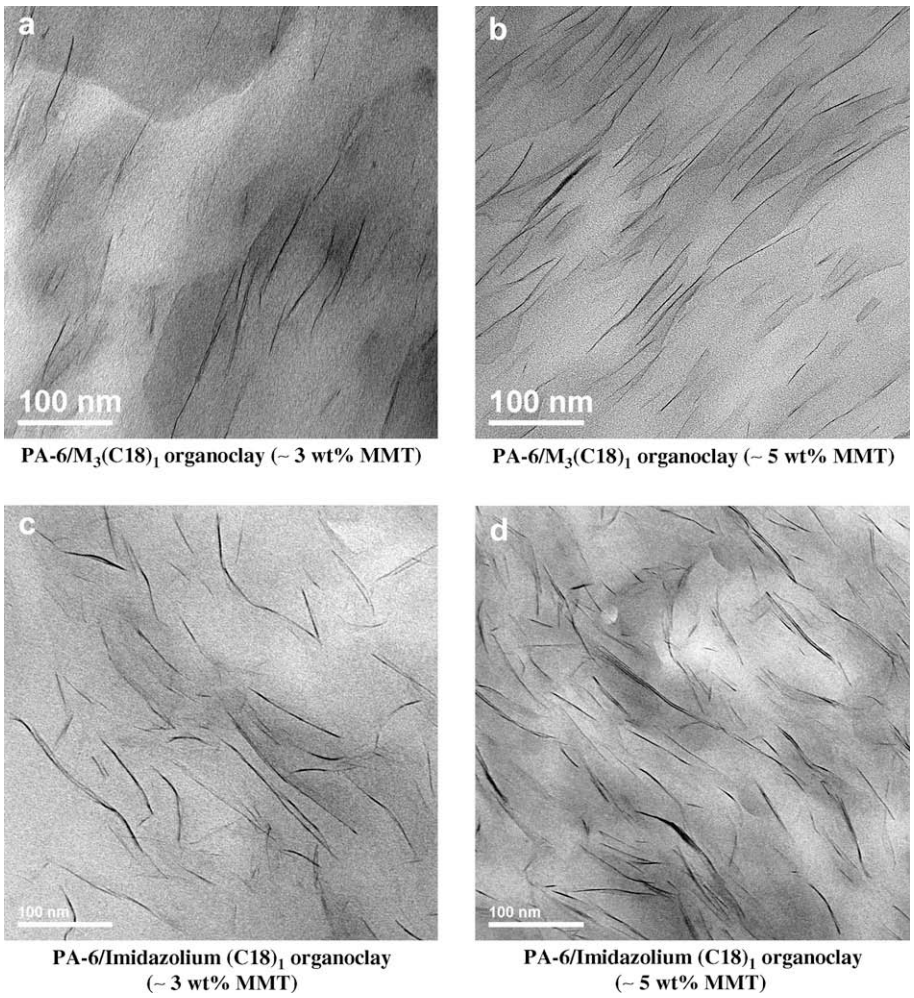

Fig. 3. TEM images of PA-6 nanocomposites based on (a) $M_3(C18)_1$ organoclay (~3 wt% MMT), (b) $M_3(C18)_1$ organoclay (~5 wt% MMT), (c) Imidazolium $(C18)_1$ organoclay (~3 wt% MMT), and (d) Imidazolium $(C18)_1$ organoclay (~5 wt% MMT). The samples were taken from the core portion of an Izod bar and viewed parallel to the transverse direction.

35 °C and three on-line detectors: differential refractive index detector (DRI) from Waters, model 2414, differential capillary viscometer (CV) and two-angle light scattering photometer (LS) included in the dual detector module Viscotek 270 (Viscotek, Houston, TX, USA). A Waters Empower™ version 2 chromatography manager with triple detection SEC option was used for data acquisition and processing.

All experiments with PA-6 containing samples were performed in 1,1,1,3,3,3-hexafluoro-2-propanol (HFIP) with 0.01 M sodium trifluoroacetate (TFA) from Sigma (St. Louis, MO, USA), which was

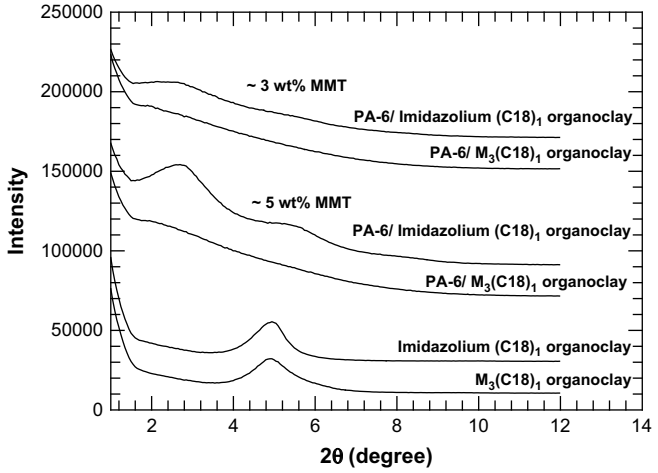

Fig. 4. WAXS scans for the $M_3(C18)_1$ and Imidazolium $(C18)_1$ pristine organoclays and PA-6-based nanocomposites containing ~3 and 5 wt% MMT. The curves are vertically offset for clarity.

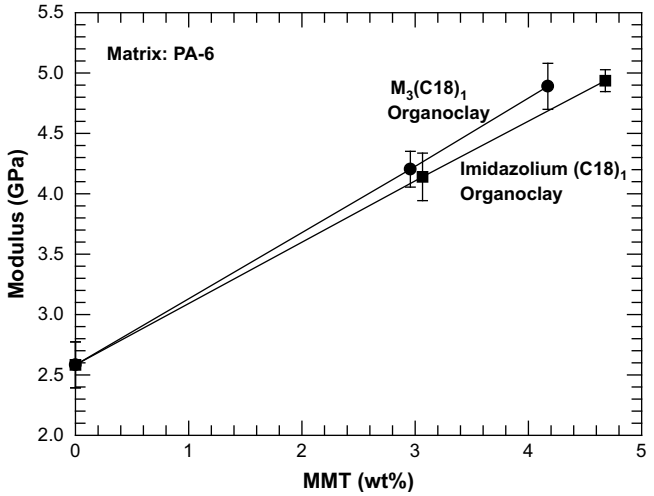

Fig. 5. Tensile modulus of PA-6 nanocomposites formed from the $M_3(C18)_1$ and Imidazolium $(C18)_1$ organoclays.

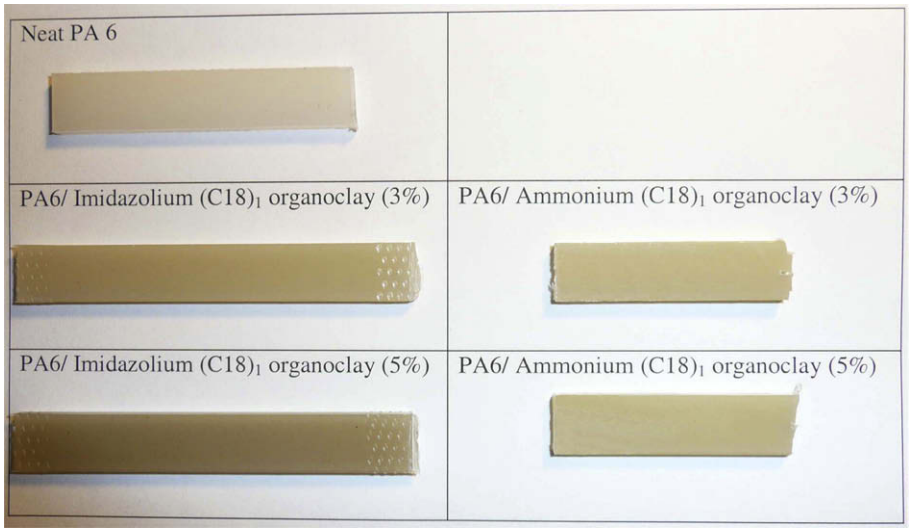

Fig. 6. Visual comparison of the color formation of PA-6 nanocomposites formed from the $M_3(C18)_1$ and Imidazolium $(C18)_1$ organoclays.

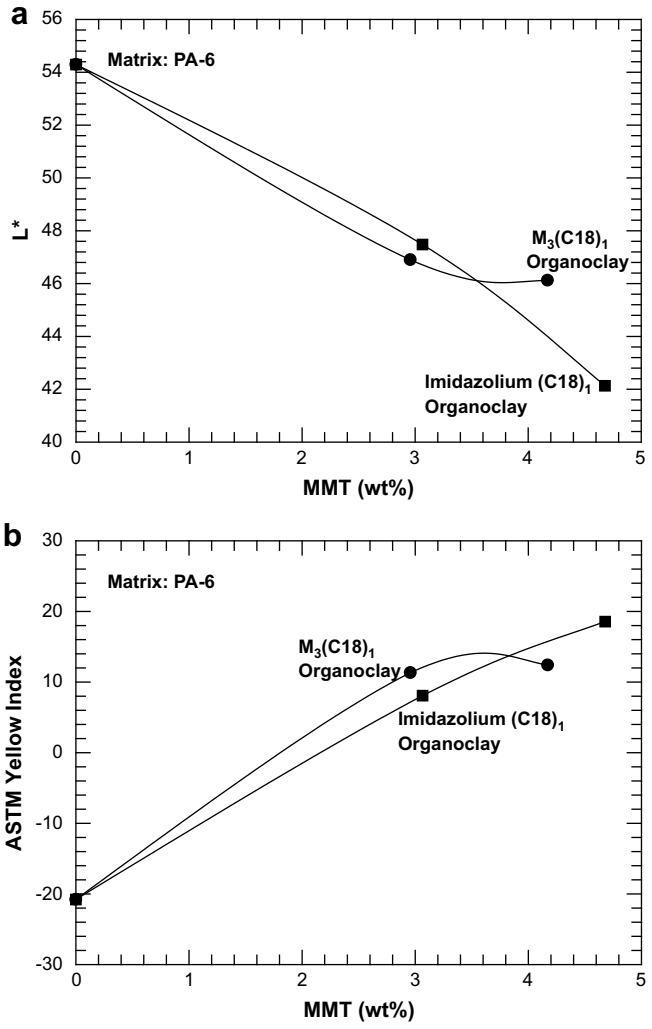

Fig. 7. Comparison of the color formation by colorimeter measurements of PA-6 nanocomposites formed from the $M_3(C18)_1$ and Imidazolium $(C18)_1$ organoclays: (a) darkness, L^*, and (b) ASTM yellow index.

used both as a mobile phase and a sample solution. A column set consisting of three styrene–divinylbenzene Shodex columns (JM Science, Grand Island, NY, USA), two GPC HFIP-806M™ with exclusion limit 2×10^7 and one Shodex GPC HFIP-804M™ with exclusion limit 2×10^5, was used for all separations in HFIP. For the PC-based nanocomposites, tetrahydrofuran (THF) stabilized with 0.025% 2,6-di-tert-butyl-4-methylphenol from J.T Baker, Phillipsburg, NJ, USA, was used as a mobile phase and a sample solution, together with a set of three styrene–divinylbenzene columns from Polymer Laboratories (Church Stretton, UK): two PL Gel Mixed C linear columns and one PL Gel 500A column with exclusion limits similar to those used in the HFIP experiments.

The samples (both neat polymers and nanocomposites) were prepared at 2 mg/mL concentration in the mobile phase solvent with 4 h allowed for dissolution at room temperature with moderate agitation using automatic sample preparation system PL 260™ from Polymer Laboratories. All sample solutions were passed through a 0.45 μm PTFE membrane filter prior to injection.

The triple detection data reduction method was used to calculate molecular weight distribution (MWD), average molecular weights and intrinsic viscosity ($[\eta]$) without column calibration. The detail description of the method including the incorporated customized algorithm is published elsewhere [26].

2.3.6. Dilute solution viscosity measurements

Viscosity was determined for dilute solution of dried extruded PA-6 pellets in *m*-cresol at concentration 0.4 g/dL using a size 200

Table 2
Average molecular weights and intrinsic viscosity of PA-6 determined by multi-detector SEC in HFIP.

Sample	$\overline{M}_n$ (g/mol)	$\overline{M}_w$ (g/mol)	$\overline{M}_z$ (g/mol)	PDI	$[\eta]$ (dL/g)
As-received PA-6	29,900	59,500	88,900	1.99	2.4
Extruded PA-6	28,100	56,000	82,000	1.99	2.3
PA-6/$M_3(C18)_1$ organoclay (~3 wt% MMT)	35,200	74,900	124,000	2.35	2.1
PA-6/$M_3(C18)_1$ organoclay (~5 wt% MMT)	31,300	66,600	106,000	2.38	2.4
PA-6/Imidazolium $(C18)_1$ organoclay (~3 wt% MMT)	29,900	70,200	122,000	2.13	2.5
PA-6/Imidazolium $(C18)_1$ organoclay (~5 wt% MMT)	33,100	78,700	139,000	2.13	2.4

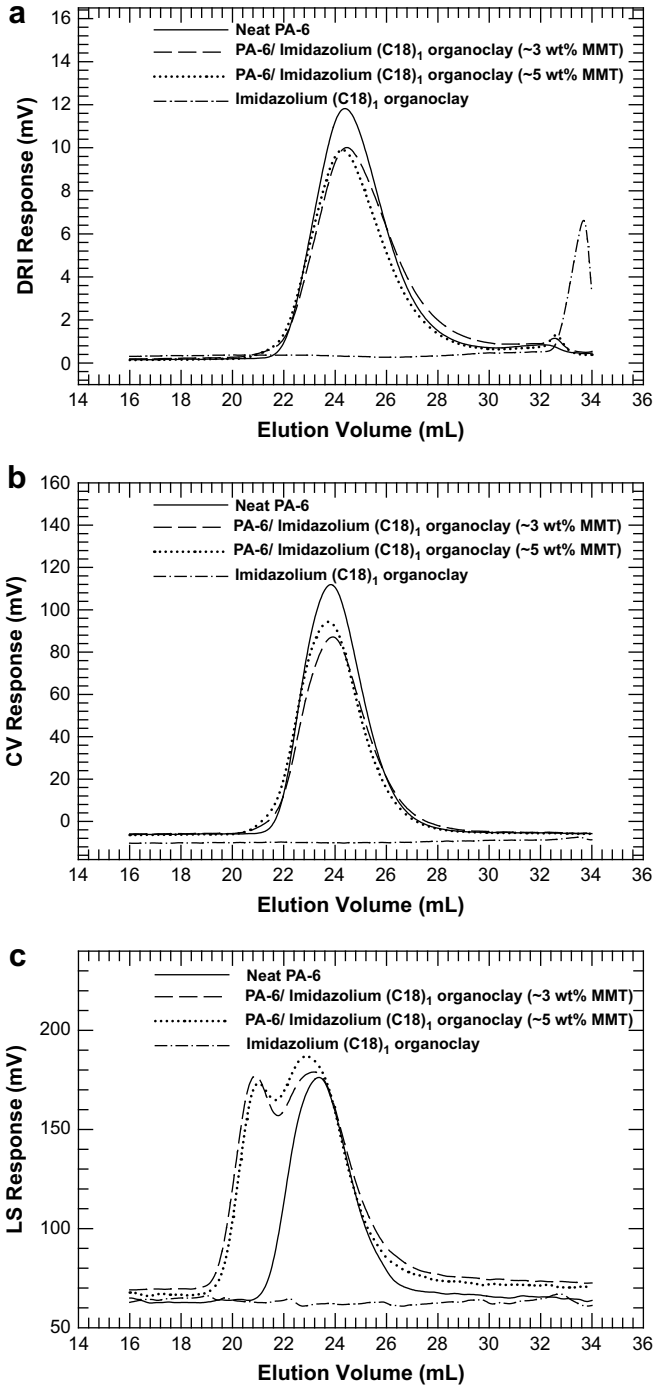

Fig. 8. SEC traces, (a) DRI, (b) CV, and (c) LS at 90° scattering angle, of extruded PA-6 and PA-6 nanocomposites formed with Imidazolium $(C18)_1$ organoclay.

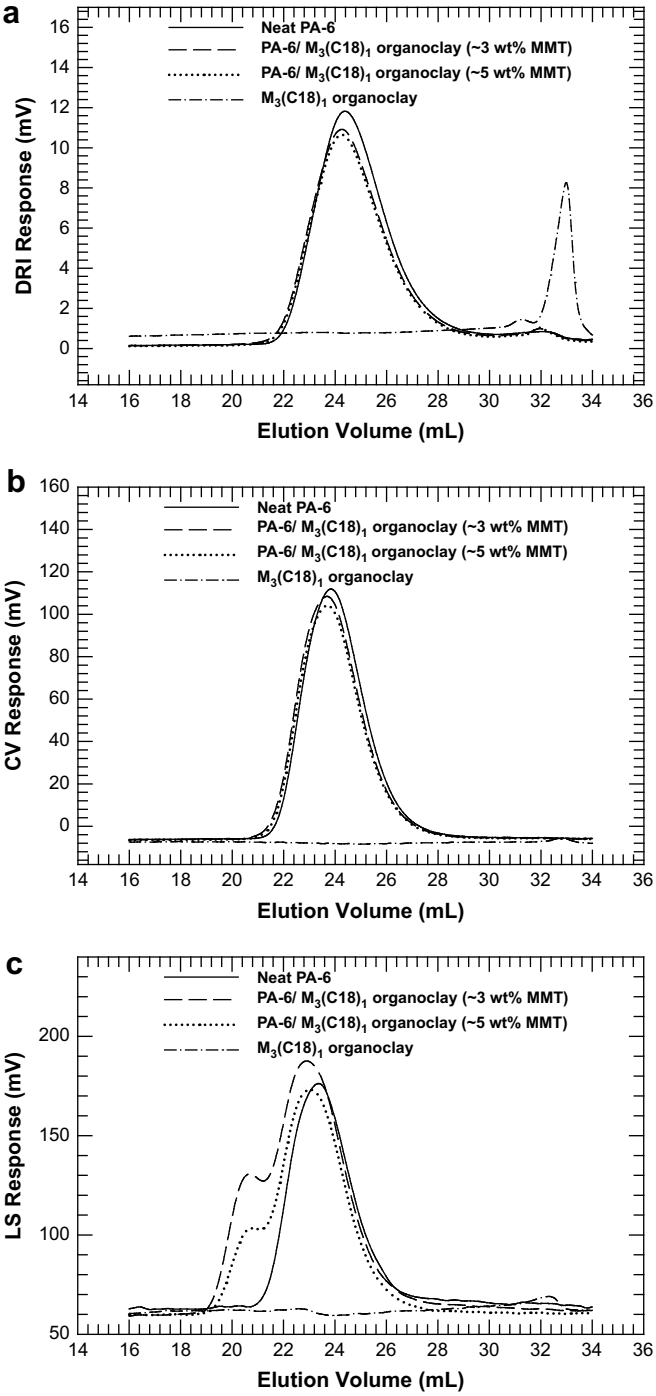

Fig. 9. SEC traces, (a) DRI, (b) CV, and (c) LS at 90° scattering angle, of extruded PA-6 and PA-6 nanocomposites formed with $M_3(C18)_1$ organoclay.

Cannon–Fenske viscometer (ASTM D446) at 25 °C. An intrinsic viscosity, $[\eta]$, was calculated by the Solomon–Ciuta equation [27,28]:

$$[\eta] = \{2[(t/t_0) - \ln(t/t_0) - 1]\}^{0.5}/c \quad (1)$$

where c is the concentration of the solution, t is the flow time of solution and t_0 is the flow time of pure solvent. Similar measurements were conducted on unfiltered dispersions of PA-6-based nanocomposites in *m*-cresol assuming that clay has a negligible effect on the polymer solution viscosity [2]. The approximate viscosity-average molecular weight, $\overline{M}_v$, for each sample was calculated from the intrinsic viscosity value using Mark–Houwink equation for PA-6 in *m*-cresol with parameters derived in [29]:

$$[\eta] = 5.26 \times 10^{-4}\ \overline{M}_v^{0.745} \quad (2)$$

3. Results and discussion

3.1. Thermal stability of organoclays

The degradation of the organoclays was monitored by thermogravimetric analysis, TGA, using both temperature sweep and

Table 3
Viscosity-average molecular weight of PA-6 determined from intrinsic viscosity in *m*-cresol.

Sample	$\overline{M}_v$ (g/mol)	$\overline{M}_v$ Reduction(%)
Extruded PA-6	58,300	–
PA-6/$M_3(C18)_1$ organoclay (~3 wt% MMT)	55,400	5.0
PA-6/Imidazolium $(C18)_1$ organoclay (~3 wt% MMT)	55,000	5.7

isothermal runs; results are shown in Fig. 2. The signals from the TGA have been scaled to represent the weight percent remaining of the surfactant originally on the organoclay, since the inorganic aluminosilicate remains stable and its weight will not change during the tests at the temperatures used. As expected, the differences in the thermal stability of these two organoclays are quite remarkable. The surfactants used to form the two organoclays both have one long alkyl tail; however, the cations are of imidazolium and ammonium-types, respectively. Obviously, the organoclay modified by the imidazolium-based surfactant is far more thermally stable than that from the ammonium-based surfactant. Fig. 2(a) clearly shows that the imidazolium-type organoclay begins to decompose at 300 °C; whereas, at this temperature, the ammonium-type organoclay has already lost about 20% of its surfactant weight. Fig. 2(b) and (c) offer obvious proof of their dramatically different thermal behavior from another perspective. Isothermal runs at two different temperatures, 240 °C and 260 °C, which are the melt processing temperatures for PA-6 and PC nanocomposites, respectively, were performed on the two organoclays over the course of 10 min, which is the residence time used to melt process these nanocomposites. The results clearly show significant differences in the thermal stability of these two organoclays. After 10 min at 240 °C, the imidazolium organoclay has only lost about 1% of its surfactant, while the ammonium organoclay lost more than 10%. The results shown in Fig. 2(c) reveal even more remarkable differences at the elevated test temperature (260 °C), with the imidazolium-type organoclay still retaining 98% of its surfactant and the ammonium-type organoclay losing almost 20% of its surfactant in 10 min.

3.2. PA-6 nanocomposites

3.2.1. Morphology

Properly prepared TEM images offer the most direct visualization of the dispersion of the clay particles in nanocomposites. Fig. 3 compares the morphology of PA-6 nanocomposites based on both ammonium and imidazolium organoclays. Fairly well-exfoliated morphologies can be observed in all the PA-6 nanocomposites. With closer examinations of these TEM images, some differences in the organoclay exfoliation can be detected. Most of the particles in the nanocomposites formed from ammonium-type organoclay are single platelets, while for the imidazolium

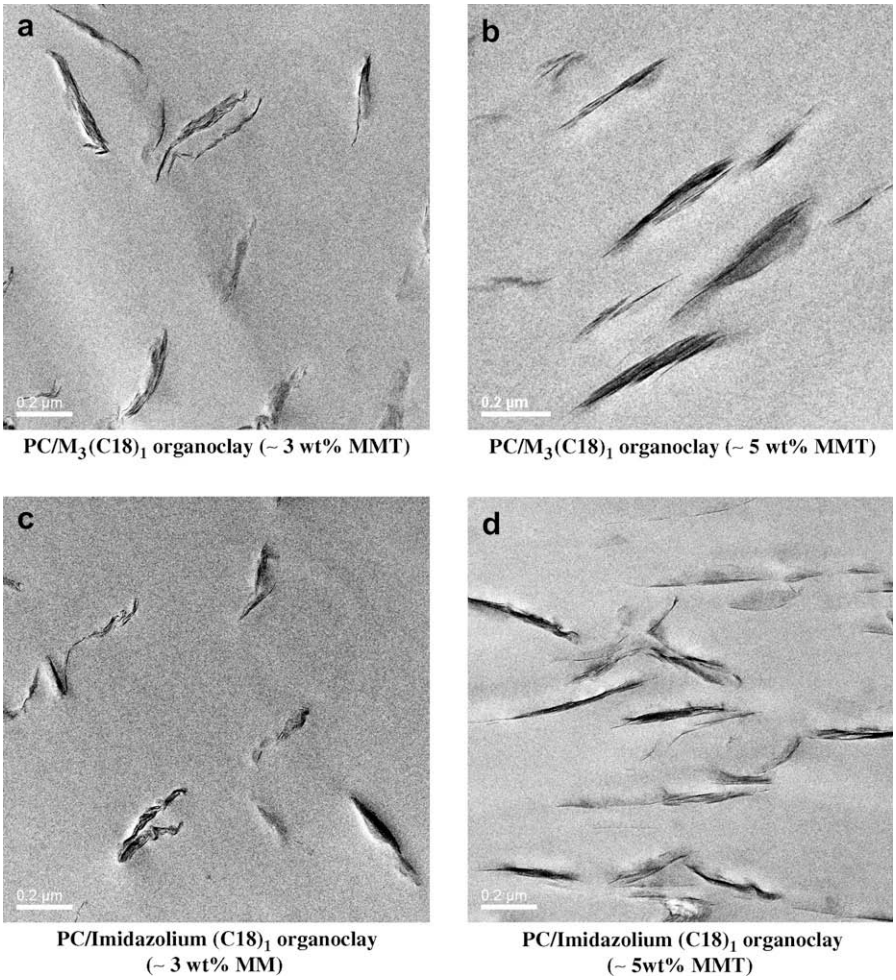

Fig. 10. TEM images of PC nanocomposites based on (a) $M_3(C18)_1$ organoclay (~3 wt% MMT), (b) $M_3(C18)_1$ organoclay (~5 wt% MMT), (c) Imidazolium $(C18)_1$ organoclay (~3 wt% MMT), and (d) Imidazolium $(C18)_1$ organoclay (~5 wt% MMT). The samples were taken from the core portion of an Izod bar and viewed parallel to the transverse direction.

Table 4
Particle analysis results on PC nanocomposites.

PC nanocomposites (~5 wt% MMT)	Organoclay used	
	$M_3(C18)_1$ organoclay	Imidazolium $(C18)_1$ organoclay
Particle length, $\bar{l}_n$ (nm)	590	404
Particle thickness, $\bar{t}_n$ (nm)	31.6	20.6
Aspect ratio, $\bar{l}_n/\bar{t}_n$	9.33	9.79
Total area analyzed (μm^2)	32.6	32.6
Particle density (particles/μm^2)	10	14

organoclay, some thin stacks of platelets can be observed along with the single platelets.

The WAXS scans of these PA-6 nanocomposites prepared from the imidazolium and ammonium organoclays are shown in Fig. 4; scans for neat organoclays are also included for comparison. The scans for the two organoclays show very similar patterns, and their characteristic basal peaks are at almost the same position, suggesting similarly expanded clay galleries after the cationic exchange with either the ammonium or the imidazolium cation. The scans of the nanocomposites containing various MMT loadings corroborate what is seen in the TEM images. For PA-6/$M_3(C18)_1$ organoclay nanocomposites, only slight hints of curvature can be observed at very low angles, suggesting a fairly well-exfoliated morphology. For PA-6/Imidazolium $(C18)_1$ organoclay nanocomposites, broad peaks at lower angles with respect to those shown by neat organoclays can be clearly seen especially for the nanocomposite with higher MMT loading (~5 wt% MMT); these features are indicative of not fully exfoliated stacks of clay platelets.

The slightly poorer organoclay exfoliation observed in PA-6/Imidazolium $(C18)_1$ organoclay nanocomposites might be attributed to the difference in size and charge density or charge distribution of the imidazolium cation compared to the ammonium cation; the larger imidazolium cations cover more of the silicate surfaces, which reduces the beneficial interactions between the polar PA-6 polymer and hydrophilic silicate platelets [12,30,31]. This line of reasoning is consistent with our experience with a variety of surfactant structures; however, at the present time, this should be regarded as only a reasonable hypothesis. The nature of the charge may affect the interaction with the platelet surface and the polymer.

3.2.2. Modulus

The moduli of these PA-6 nanocomposites formed from the ammonium $M_3(C18)_1$ and imidazolium $(C18)_1$ organoclays are plotted versus MMT content in Fig. 5. The addition of organoclay to the PA-6 matrix produces significant increase in modulus for both types of organoclay. The nanocomposites based on the $M_3(C18)_1$ organoclay show slightly higher moduli than those based on the imidazolium $(C18)_1$ organoclay at various clay loadings. This result is consistent with the results shown by TEM and WAXS, since better exfoliation usually leads to higher level of reinforcement.

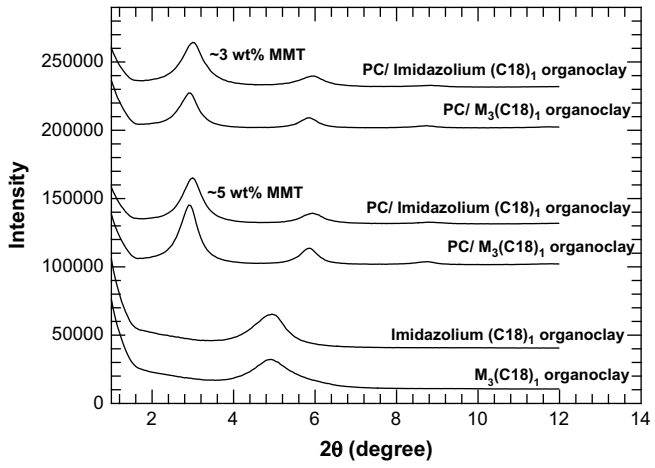

Fig. 11. WAXS scans for the $M_3(C18)_1$ and Imidazolium $(C18)_1$ pristine organoclays and PC-based nanocomposites containing ~3 and 5 wt% MMT. The curves are vertically offset for clarity.

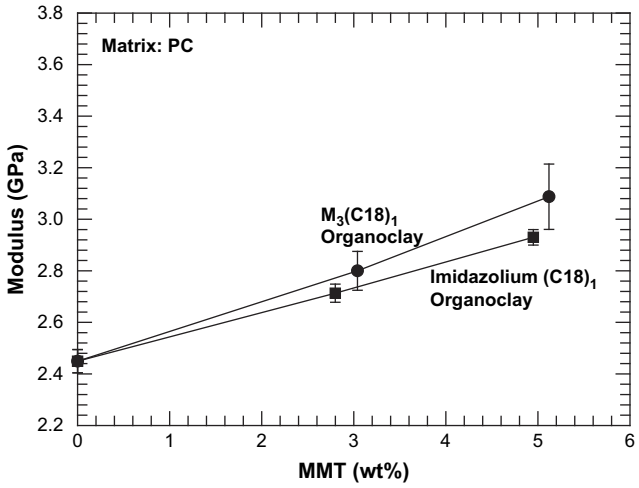

Fig. 12. Tensile modulus of PC nanocomposites formed from the $M_3(C18)_1$ and Imidazolium $(C18)_1$ organoclays.

3.2.3. Color formation

Generally more intense color formation, i.e., darker and more yellow, suggests more severe degradation of the polymer matrix, organoclay, or the combination thereof [2,4,15,17,18,32,33]. Fig. 6 visually shows the color of PA-6 nanocomposites formed from the two organoclays, and Fig. 7(a) and (b) quantitatively documents the color of each nanocomposite. In general, the depth of color and the yellowness determined visually show good correlations with the L^* and yellowness index (YI) values, respectively. As expected, nanocomposites with higher MMT loadings show darker and more yellow color as observed visually and indicated by lower L^* values and higher YI values; however, the nanocomposites with the same clay loading formed from the two organoclays show very similar color in both darkness and yellowness.

3.2.4. Molecular weight determination

A multidetector SEC method was utilized to analyze molecular structure of the PA-6 matrix in these nanocomposites. This method allows for direct measurement of molecular weight and intrinsic viscosity of the separated fractions without need for column calibration but requires an accurate value of refractive index increment, dn/dc, of the polymer in HFIP used as a mobile phase and a sample solution. We found $dn/dc = 0.235$ using the area under the DRI chromatogram for neat PA-6, which is close to the published value [34]. The same value was applied to all PA-6 nanocomposites, which were filtered prior to injection. A small amount of sodium TFA was added to HFIP to avoid non-size-exclusion effects reported in the literature [34].

The calculated average molecular weights, polydispersity index (PDI $= \overline{M}_w/\overline{M}_n$) and intrinsic viscosity, [η], measured by SEC in HFIP are summarized in Table 2. One can see that the molecular weight of PA-6 is slightly reduced when neat PA-6 is processed in the DSM Microcompounder at 240 °C for 10 min. As the polydispersity of the polymer did not change, we can assume that a very slight random chain scission hydrolysis reaction took place in the compounder. However, after melt mixing with the organoclays, the

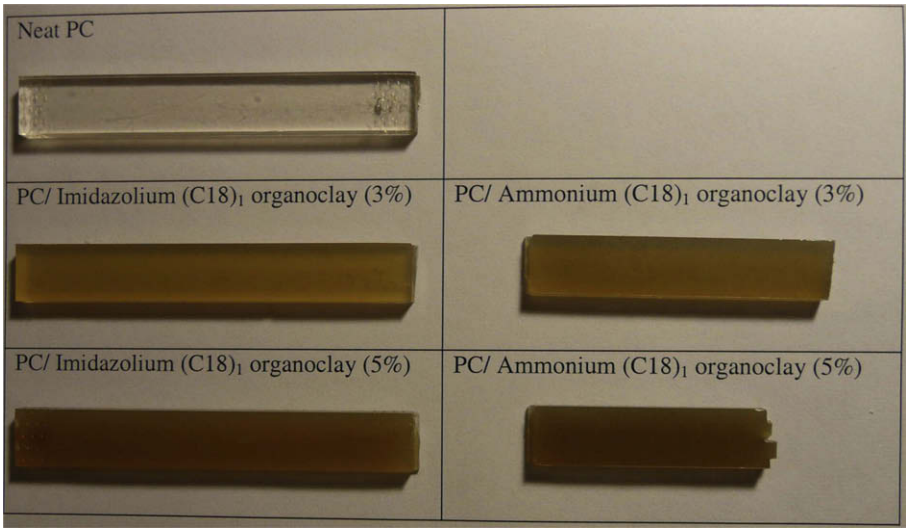

Fig. 13. Visual comparison of the color formation of PC nanocomposites formed from the $M_3(C18)_1$ and Imidazolium $(C18)_1$ organoclays.

calculated polymer molecular weights as well as polydispersity substantially increased with respect to that of the extruded neat polymer, without any noticeable changes of intrinsic viscosity. This observation clearly indicates the presence of branched structures in the dissolved polymer nanocomposites and is confirmed by the shape of the individual traces from the different detectors shown at Figs. 8 and 9. Thus, all three detector responses are proportional to the concentration of the separated fractions, but the LS response is also proportional to the molecular weight, and the CV response is proportional to intrinsic viscosity (size) of the macromolecules [26]. The appearance of an additional, lower elution time (high-molecular weight) peak at the light scattering traces (ca. 20 mL elution volume) of PA-6 nanocomposites indicates some very high-molecular weight fractions absent in the extruded neat polymer as well as in the organoclays which were dispersed in HFIP, filtered and injected in the SEC system for comparison (an additional peak at the DRI trace at 34 mL elution volume is most probably caused by the residual surfactant not attached chemically to the clay particles). These branched (crosslinked) structures are highly dense and have lower concentration in solution which explains why they are practically not seen in the DRI and CV chromatograms, and while they significantly increase the observed molecular weight (especially z-average molecular weight, $\overline{M}_z$), they do not affect the intrinsic viscosity of the solution or can make it even smaller due to reduction in size of branched macromolecules (see Table 2). This observation was confirmed also by the solution viscosity measurements of PA-6 nanocomposites in *m*-cresol. The results shown in Table 3 reveal only a very slight decrease (less than 6%) in the apparent $\overline{M}_v$ value for the PA-6 in the nanocomposites as compared to that of the extruded neat PA-6.

The branched structures observed in the PA-6 nanocomposites, even in very dilute solution used for the SEC experiments, most probably contain small exfoliated nanoclay particles as branched points, and are stable even in a very strong solvent such as HFIP. The PA-6 nanocomposites have a very well-exfoliated morphology, which offers large interfacial area between the polymer matrix and the aluminosilicates or various amine surfactants. If any of the components, either the silicate platelets or the surfactant molecules, have the potential of causing branching or crosslinking type behavior, these effects will be exaggerated in these well-exfoliated PA-6 nanocomposites. It is obvious that in the SEC experiments we can see only a small portion of the branched structures with submicron size, while the majority of them, together with chemically non-bound nanoclay, are either filtered out prior to injection or are trapped in the columns or the column frits. It might be speculated that such structures contribute to the observed increase in tensile modulus for both types of organoclays. Note that similar branched structures were previously reported for polyester/silica nanocomposites [28].

The SEC and viscosity measurements of melt blended PA-6 nanocomposites did not reveal a noticeable reduction in polymers molecular weight reported previously for surfactants containing various levels of unsaturation [2,35]. The surfactants used here contain saturated hydrocarbon tails and the melt processing was conducted under nitrogen protection, which significantly reduces the degradation through thermal and oxidation routes compared to surfactants containing unsaturated carbon bonds. It has been reported that the free radicals generated through the thermo-oxidation of the double bonds can attack the polymer, which may result in chain scission and, hence, a reduction in polymer molecular weight [2]. The effect of some possible degradation of the PA-6 matrix may also be compensated by aforementioned crosslinking reaction initiated by the imidazolium $(C18)_1$ or $M_3(C18)_1$ organoclays.

3.3. Polycarbonate nanocomposites

3.3.1. Morphology

TEM images of the PC nanocomposites formed from the two organoclays are compared in Fig. 10. Unlike PA-6 nanocomposites, relatively large organoclay particles containing many aluminosilicate platelets can be observed in all the PC nanocomposites, indicating rather poor exfoliation of the organoclays. Simple visual inspection of these images obtained from nanocomposites based on various organoclays does not reveal significant differences. A quantitative particle analysis of these images using similar methods as described previously [31,36,37] was conducted for each sample with the results summarized in Table 4. The clay particles in the PC/$M_3(C18)_1$ organoclay mixture are larger on average in both length and thickness, and the density of particles is lower, than for the PC/Imidazolium $(C18)_1$ organoclay mixture. The aspect ratios of the particles are quite similar, but the imidazolium $(C18)_1$ organoclay particles have a slightly higher value. The smaller particle length and thickness but higher particle density and aspect ratio are quantitative indicators of better organoclay dispersion and exfoliation in nanocomposites. Based on this analysis, it appears the

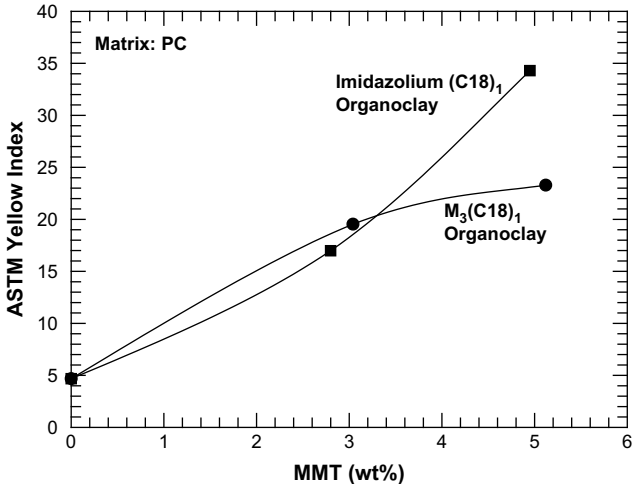

Fig. 14. Comparison of the ASTM yellow index by colorimeter measurements of PC nanocomposites formed from the $M_3(C18)_1$ and Imidazolium $(C18)_1$ organoclays.

imidazolium $(C18)_1$ organoclay leads to slightly better exfoliation in PC than does the $M_3(C18)_1$ organoclay.

Fig. 11 shows the WAXS scans for the PC nanocomposites with the scans of neat organoclays included for comparison. All the PC nanocomposites prepared in this study reveal distinctive multiple peaks. The d_{001} peaks all largely shifted to the left, higher d spacing, as compared to the peak positions of corresponding organoclays, indicating that there is some intercalation into the organoclay galleries but exfoliation is much poorer than seen in PA-6. These results agree very well with the morphologies observed by TEM. It is interesting to note that secondary reflections only appear in X-ray scans of nanocomposites, not in those of the neat organoclays. This may be attributed to the better particle alignment in nanocomposites, realized during the injection molding [30].

3.3.2. Modulus

Tensile moduli were measured for the PC nanocomposites formed from both the ammonium and the imidazolium organoclays with the results shown in Fig. 12. As expected, addition of organoclay increases the moduli of these materials. Interestingly, the moduli of the PC/$M_3(C18)_1$ organoclay nanocomposites are slightly higher than those of the PC/Imidazolium $(C18)_1$ organoclay nanocomposites, which is opposite to our expectation based on the better exfoliation achieved in PC/Imidazolium $(C18)_1$ organoclay nanocomposites.

3.3.3. Color formation

The extent of color formation is documented both visually and quantitatively in Figs. 13 and 14 respectively. Simple examination by eye of the injection molded rectangular bars does not reveal significant differences. Quantitative examination using the yellowness index as an indicator shows that nanocomposites containing ~3 wt% MMT formed from the two organoclays have similar yellowness in color, while, as the clay loading gets higher, comparing nanocomposites with ~5 wt% MMT, the one formed from the imidazolium organoclay is more yellow in color.

3.3.4. Molecular weight determination

Multidetector SEC was used to determine the degradation of the polycarbonate in the neat state and in the nanocomposites. The results shown in Table 5 are significantly different from those obtained for the PA-6 nanocomposites. As seen for PA-6, the extruded virgin PC has a slightly reduced molecular weight and intrinsic viscosity compared to as-received PC. However, the matrix molecular weight and intrinsic viscosity reductions observed in the PC nanocomposites are far greater than that experienced by the extruded neat polymer; no indications of branched structures (e.g., bimodality of the LS trace or increase in molecular weight or polydispersity) were observed in the case of the PC nanocomposites. More severe molecular weight reductions are observed in PC nanocomposites formed from the imidazolium organoclay. This result might be attributed to the better exfoliation, in other words, the larger surface area of organoclay exposed to the polymer matrix, found in PC/Imidazolium $(C18)_1$ organoclay nanocomposites, since the degradation of the polycarbonate matrix is believed to stem from chemical reactions with the organoclay surface either via the degradation products of the surfactant or the metal ions in the aluminosilicate platelets [4]. In addition, the highly acidic hydrogen on the "2" position (the carbon between the two nitrogen atoms in the ring) in the imidazolium cation is active [5,38] and may lead to degradation of polycarbonate. The more severe polymer degradation (degradation byproducts and molecular weight reduction of polymer matrix) in nanocomposites formed from imidazolium $(C18)_1$ organoclay might be responsible for the slightly lower moduli observed for the nanocomposites formed from the imidazolium $(C18)_1$ organoclay than those from the PC/$M_3(C18)_1$ organoclay.

Table 5
Average molecular weights and intrinsic viscosity of PC determined by multi-detector SEC in THF.

Sample	$\overline{M}_n$ (g/mol)	$\overline{M}_n$[a] reduction (%)	$\overline{M}_w$ (g/mol)	$\overline{M}_z$ (g/mol)	PDI	$[\eta]$ (dL/g)
As-received PC	8340	–	19,000	31,400	2.28	0.34
Extruded PC	8090	–	18,800	31,300	2.33	0.33
PC/$M_3(C18)_1$ organoclay (~3 wt% MMT)	6860	15.2	15,800	26,000	2.31	0.30
PC/$M_3(C18)_1$ organoclay (~5 wt% MMT)	6060	25.2	14,100	23,700	2.33	0.28
PC/Imidazolium $(C18)_1$ organoclay (~3 wt% MMT)	5510	32.0	12,500	21,700	2.27	0.24
PC/Imidazolium $(C18)_1$ organoclay (~5 wt% MMT)	5870	27.5	13,700	22,800	2.33	0.26

[a] The reduction percentage is relative to the $\overline{M}_n$ of virgin extruded polycarbonate.

4. Summary and conclusions

Organoclays based on ammonium-type and imidazolium-type surfactants were shown to have significantly different thermal stabilities. These organoclays were also used to form PA-6 and PC nanocomposites using a DSM Microcompounder. The effects of the different chemical structure and thermal stability of these surfactants in the organoclays on the morphology and properties of the nanocomposites formed are compared. Morphology was assessed by TEM and WAXS. Tensile modulus was also used as an indicator of organoclay exfoliation. Differences in color formation and molecular weight change of the matrix polymers after melt blending with the organoclays were determined.

For PA-6, the imidazolium $(C18)_1$ organoclay resulted in slightly poorer organoclay exfoliation than the ammonium $M_3(C18)_1$ organoclay; however, this did not result in a very significant difference in the properties of the nanocomposites formed. Both organoclays form fairly well-exfoliated nanocomposites. Incorporation of organoclay in the PA-6 matrix produces only slight changes in color and an increase in polymer molecular weight due to branching reaction.

For PC nanocomposites formed from the two organoclays, only intercalated morphologies can be achieved by melt processing. Unlike the PA-6 nanocomposites, it appears that PC nanocomposites from the imidazolium $(C18)_1$ organoclay has a slightly better exfoliated structure, as suggested by the particle analysis results. However, as a trade-off for better exfoliation, the PC/Imidazolium $(C18)_1$ organoclay nanocomposites developed more intensive yellow color and the matrix polymer experienced more severe molecular weight reduction due to the increased surface area of the organoclay.

Based on the results in this study, it seems that the thermal stability of organoclays is not the key factor in organoclay exfoliation in melt processed polymer nanocomposites, since the exfoliation/dispersion process may have been completed on a time scale before the degradation of surfactant progresses to a detrimental level [36]. On the other hand, it appears that the size and geometric structure of the surfactant cations may play a significant role; it is speculated that the larger imidazolium cations cover more of the silicate surface leading to less favorable interactions between the organoclay and the polymer matrix so that the organoclay exfoliation level in PA-6 nanocomposites is reduced slightly. There is no simple direct correlation between the thermal stability of the organoclay and the molecular weight reduction of the polymer matrix. The more thermally stable imidazolium $(C18)_1$ organoclay does not lead to less molecular weight reduction of the polymer matrices either in PA-6 or PC nanocomposites.

Acknowledgements

The authors thank Mr. Tony Gonzalez at Southern Clay Products, Inc. for synthesis of the experimental organoclays and the help with the WAXS analysis.

References

[1] Cui L, Khramov DM, Bielawski CW, Hunter DL, Yoon PJ, Paul DR. Polymer 2008;49(17):3751–61.
[2] Fornes TD, Yoon PJ, Paul DR. Polymer 2003;44(24):7545–56.
[3] Shah RK, Paul DR. Polymer 2006;47(11):4075–84.
[4] Yoon PJ, Hunter DL, Paul DR. Polymer 2003;44(18):5341–54.
[5] Awad WH, Gilman JW, Nyden M, Harris RH, Sutto TE, Callahan J, et al. Thermochimica Acta 2004;409(1):3–11.
[6] Mittal V. European Polymer Journal 2007;43(9):3727–36.
[7] Gilman JW, Awad WH, Davis RD, Shields J, Harris Jr RH, Davis C, et al. Chemistry of Materials 2002;14(9):3776–85.
[8] Davis CH, Mathias LJ, Gilman JW, Schiraldi DA, Shields JR, Trulove P, et al. Journal of Polymer Science, Part B: Polymer Physics 2002;40(23):2661–6.
[9] Modesti M, Besco S, Lorenzetti A, Causin V, Marega C, Gilman JW, et al. Polymer Degradation and Stability 2007;92(12):2206–13.
[10] Wang ZM, Chung TC, Gilman JW, Manias E. Journal of Polymer Science, Part B: Polymer Physics 2003;41(24):3173–87.
[11] Fornes TD, Yoon PJ, Keskkula H, Paul DR. Polymer 2001;42(25):09929–40.
[12] Fornes TD, Yoon PJ, Hunter DL, Keskkula H, Paul DR. Polymer 2002;43(22):5915–33.
[13] Chavarria F, Paul DR. Polymer 2004;45(25):8501–15.
[14] Shah RK, Paul DR. Polymer 2004;45(9):2991–3000.
[15] Davis A, Golden JH. Nature 1965;206(4982):397.
[16] Song S-C, Lee SB, Jin J-I, Sohn YS. Macromolecules 1999;32(7):2194–203.
[17] Abbås KB. Polymer 1981;22(6):836–41.
[18] Abbås KB. Polymer 1980;21(8):936–40.
[19] Lu H-j, Liang G-Z, Ma X-y, Zhang B-y, Chen X-b. Polymer International 2004;53(10):1545–53.
[20] Huang Y, Ma XY, Liang GZ, Yan HX. Clay Minerals 2007;42(4):463–70.
[21] Chu L-L, Anderson SK, Harris JD, Beach MW, Morgan AB. Polymer 2004;45(12):4051–61.
[22] Ngo HL, LeCompte K, Hargens L, McEwen AB. Thermochimica Acta 2000;357:97–102.
[23] Cui L, Paul DR. Polymer 2007;48(6):1632–40.
[24] Yoo Y, Paul DR. Polymer 2008;49(17):3795–804.
[25] Shah RK, Cui L, Williams KL, Bauman B, Paul DR. Journal of Applied Polymer Science 2006;102(3):2980–9.
[26] Brun Y. Multiple detection in size-exclusion chromatography. ACS Symposium Series 2005;893:281–301.
[27] Solomon O, Ciuta IZ. Journal of Applied Polymer Science 1962;6(24):683–6.
[28] Bikiaris D, Karavelidis V, Karayannidis G. Macromolecular Rapid Communications 2006;27(15):1199–205.
[29] Tuzar Z, Kratochvil P. Journal of Polymer Science, Part B: Polymer Letters 1965;3:17–8.
[30] Chavarria F, Paul DR. Polymer 2006;47(22):7760–73.
[31] Cui L, Ma X, Paul DR. Polymer 2007;48(21):6325–39.
[32] Holland BJ, Hay JN. Polymer International 2000;49(9):943–8.
[33] Peebles Jr LH, Huffman MW. Journal of Polymer Science, Part A-1: Polymer Chemistry 1971;9(7):1807–22.
[34] Mourey TH, Bryan TG. Journal of Chromatography A 2002;964(1–2):169–78.
[35] Davis RD, Gilman JW, VanderHart DL. Polymer Degradation and Stability 2003;79(1):111–21.
[36] Cui L, Hunter DL, Yoon PJ, Paul DR. Polymer 2008;49(17):3762–9.
[37] Dennis HR, Hunter DL, Chang D, Kim S, White JL, Cho JW, et al. Polymer 2001;42(23):9513–22.
[38] Carlin RT, Fuller J. Molten salts: from fundamentals to applications. Dordrecht: Kluwer Academic Publishers; 2002. p.321.